Accepted Manuscript

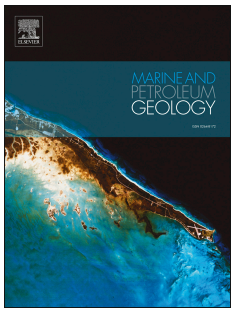

The Challenges of Quantifying the Carbon Stored in Arctic Marine Gas Hydrate

Héctor Marín-Moreno, Michela Giustiniani, Umberta Tinivella, Elena Piñero

PII: S0264-8172(15)30137-9

DOI: 10.1016/j.marpetgeo.2015.11.014

Reference: JMPG 2396

To appear in: *Marine and Petroleum Geology*

Received Date: 19 November 2015

Accepted Date: 21 November 2015

Please cite this article as: Marín-Moreno, H., Giustiniani, M., Tinivella, U., Piñero, E., The Challenges of Quantifying the Carbon Stored in Arctic Marine Gas Hydrate, *Marine and Petroleum Geology* (2015), doi: 10.1016/j.marpetgeo.2015.11.014.

The Challenges of Quantifying the Carbon Stored in Arctic Marine Gas Hydrate

Héctor Marín-Moreno[1,2*], Michela Giustiniani[1], Umberta Tinivella[1] and Elena Piñero[3]

[1]Istituto Nazionale di Oceanografia e di Geofisica Sperimentale, Trieste, Italy

[2]National Oceanography Centre, European Way, Southampton, SO14 3ZH, UK

[3]Barcelona Center for Subsurface Imaging, Institut de Ciències del Mar-CSIC, E-08003 Barcelona, Spain

[*]Corresponding author email: hector.marin.moreno@noc.ac.uk

[*]Corresponding author number: 00447748860231

Highlights

- The amount of carbon stored in hydrate below the Arctic Ocean remains uncertain
- A function for the fluid flow that gives observed hydrate saturations is proposed
- Arctic marine gas hydrates likely form by upwards-advection of carbon-rich fluids
- Equivalent fluid flows of 0.02-0.04 cm yr^{-1} result in hydrate saturations of 5-10%

Abstract

The quantification of the carbon stored in gas hydrate (GH) bearing marine sediments still remains a challenge. Despite recent efforts to develop approaches to better estimate the GH inventory globally, these estimates are still highly unconstrained due to insufficient field data and poor understanding of the mechanisms fuelling the GH stability zone (GHSZ). Here we use geophysically-derived GH saturations to constraint estimates of model-derived Arctic marine GH inventory at present. We also estimate the potential carbon released from GH dissociation under a seabed warming of 2°C over 100 yr. We estimate an inventory ranging between 0.28-541 Gt of C, which upper bound results in average GH saturations of 0.25%. Our upper bound is mainly controlled by our imposed upwards carbon-rich fluid flow of 0.01 cm yr^{-1} and it is five times greater than the most recent estimate that only considers in-situ degradation of particulate organic carbon (POC). To obtain the seismically-inferred GH saturations of 5-10% offshore west of Svalbard and in the Beaufort Sea, an upwards advection of carbon-rich fluids equivalent to 0.02 to 0.04 cm yr^{-1} is required. This mechanism may be the most important source of carbon reaching the GHSZ in Arctic marine sediments. A 2°C seabed temperature increase over 100 yr may reduce the GH inventory by about 88.44% (0.7 Gt C) if POC is the only source, and by about 5.4% (29.7 Gt C) if the main source of carbon is the upwards advection of carbon-rich fluids.

Keywords: Gas hydrate inventory, uncertainty, carbon-rich fluids, ocean warming, Arctic.

1. Introduction

At present, various countries (USA, Canada, Japan, India, China, South Korea) have important R&D programs to make gas hydrate (GH) exploitation economically feasible in the relatively near future. Therefore, the first step to understand the potentiality of hydrate as an energy resource or as a future impact to the climate is to quantify its inventory, which still is highly uncertain.

Recent global estimates of the total carbon stored in GH bearing sediments range between ~500 and 3000 Gt of which 116 Gt may be stored in the Arctic (e.g., Kretschmer et al., 2015). Hydrates are most sensitive to ocean warming at high latitudes and in shallow water depths (e.g., Hunter et al., 2013), and for a 100 yr warming period the Arctic presents the maximum absolute methane released from hydrate dissociation with a global contribution of 39% (140±10 Mt C; Kretschmer et al., 2015). However, Kretschmer et al. (2015) do not consider the upward advection of deep methane-rich fluids into the GH stability zone (GHSZ) from processes other than mechanical compaction, such as dewatering, which may significantly increase the present day GH inventory and associated future methane release. Besides, the

transformation of their estimates into GH saturation results in much smaller saturations than those inferred from seismic and controlled sourced electromagnetic (CSEM) data in several Arctic locations (e.g., Andreassen et al., 1997; Chabert et al., 2012; Goswami et al., 2015).

Uncertainties in the parameters controlling the thickness of the GHSZ (pressure, seabed temperature, geothermal gradient, salinity and phase boundary) and in the type of carbon sources and amount of carbon reaching the GHSZ result in a large range of possible estimates of the total carbon stored in GH. Here, we illustrate the influence of uncertainties in the parameters controlling the thickness of the GHSZ by considering a rather large perturbation of ±30% in the calculation of the Arctic marine GH inventory from published state-of-the-art transfer functions (Wallmann et al., 2012; Piñero et al., 2013). We also present an analysis where some of these estimates are constrained with GH saturations derived from geophysical data and propose an explicit function that allows the estimation of an equivalent upward fluid flow of methane-rich fluids into the GHSZ required satisfying geophysically-derived saturations. This function can be used anywhere when the accumulation of particulate organic carbon is not sufficient to explain average hydrate saturations above 1%. We finally assess the potential GH-derived carbon that could be released under a 2°C seabed warming scenario over 100 yr for different present-day Arctic GH inventories.

2. Methodology

The carbon stored in Arctic marine GHs was calculated using the transfer functions proposed by Wallmann et al. (2012) for diffusive-controlled geological systems, and for fully compacted and steady state compacted sediments. To consider other possible sources of dissolved methane into the GHSZ, Piñero et al. (2013) transfer function (Eq. 1) was also applied. These transfer functions are fitting equations to the numerical results from a reactive transport code that considers the dominant physical and biogeochemical processes and parameters including: sediment compaction, the solubility of methane in pore water, the formation and dissociation of GH and formation and dissolution of free methane gas in pore water, diffusive and advective transport of dissolved constituents, input and degradation of particulate organic carbon (POC) and particulate organic nitrogen (PON) via sulfate reduction and methanogenesis, anaerobic oxidation of methane (AOM), and formation and adsorption of ammonium, dissolved inorganic carbon (DIC) and methane (Piñero et al., 2013). The input parameters for the transfer functions are: (i) thickness GHSZ (H_{GHSZ}, m), (ii) sedimentation rate (SR, cm kyr^{-1}), (iii) POC (wt %), and (iv) upward advective fluid flow from mechanisms other than mechanical compaction (FF, cm yr^{-1}).

$$m_C = \sum_{n}^{N} \begin{Bmatrix} \left[\left[\left(c1 \cdot H_{GHSZ}^{c2}\left(c3 - \frac{1}{SR}\right) \cdot \left(POC + c4 \cdot FF^{c5}\right) POC^{c6}\right) \cdot A\right]; & FF \geq 0.0001SR\left(2 + \ln\left[POC\right]\right) \\ \left[\left[\left(m_C^* \cdot c7 \cdot 10^{-8} H_{GHSZ}^{c8}\left(1 - \frac{1}{SR}\right) FF \cdot POC^{c9}\right) \cdot A\right]; & FF < 0.0001SR\left(2 + \ln\left[POC\right]\right) \end{Bmatrix}_n \quad (1)$$

In Eq. (1) m_C (kg) is the total carbon locked in GH, N is the number of model cells, m_C^* (kg m^{-2}) is the carbon locked in GH per m^2 of seabed area calculated using Wallmann et al. (2012) transfer function for steady-state compaction, A (m^2) is the seabed area, and the fitting coefficients are: [*c*1=0.024; *c*2=1.587; *c*3=0.0224; *c*4=266084; *c*5=2.75; *c*6=0.063; *c*7=0.003; *c*8=4.68; *c*9=2.31]. Please note that the ascent of free methane gas, which may be another source for methane in the GHSZ, is not considered in these functions.

2.1 Volume of the GHSZ

To calculate the present-day volume of the marine GHSZ in the Arctic under steady state conditions, bathymetry, seabed temperature and geothermal gradient data were collected (Figure 1), and water salinity and gas composition were assumed. The bathymetric data was obtained from The International Bathymetric Chart of the Arctic Ocean (IBCAO) project (*http://www.ngdc.noaa.gov/mgg/bathymetry/arctic/ downloads.html*), the seabed temperature data from The National Oceanographic Data Centre website (*http://www.nodc.noaa.gov/cgi-bin/OC5/WOA09/ woa09.pl*), and the geothermal gradient data from The Global Heat Flow Database of the International Heat Flow Commission (*http://www.heatflow.und.edu/index2.html*). Note that, since we directly use geothermal gradient data, we do not need to assume any thermal conductivity value, which is normally an uncertainty source (e.g. Burwicz et al., 2011; Piñero et al., 2013). A value of 3.5 wt% Arctic Ocean salinity (Talley et al., 2011) and Structure I pure methane hydrate were assumed, the later based on other hydrate-related studies in the Arctic (e.g., Marín-Moreno et al., 2015) and because methane hydrate makes the 80% of the total inventory of naturally occurring GHs (Kvenvolden, 1993). We consider a model resolution of 2500x2500 m^2 and the above datasets were interpolated and extrapolated to that resolution. In each model cell, the thickness of the GHSZ was given by the distance between the seabed and the intersection of the cell's temperature structure (obtained using the cell's seabed temperature and geothermal gradient) with six different methane hydrate phase boundaries: (1) and (2) Dickens and Quinby-Hunt (1994; 1997), (3) Distribution Coefficient Method or K_{vsi}-Method (Sloan and Koh, 2008), (4) Moridis et al. (2008), (5) Tischenko et al. (2005) and (6) Lu and Sultan (2008). Water depth was converted to hydrostatic pressure assuming a constant water density of 1046 kg m^3 (Giustiniani et al., 2013). Sloan and Koh's (2008) and Moridis' (2008) curves are defined for pure water and Dickens and Quinby-Hunt (1994) for 3.35 wt% salinity. These GH stability

curves were converted to 3.5 wt% salinity curves using the relationship from Dickens and Quinby-Hunt (1997). For the conversion, we assumed a pure water fusion temperature of 273.2 K, a pure water fusion enthalpy of 6008 J mol^{-1}, an enthalpy of GH dissociation of 54200 J mol^{-1}, a hydration number of 6 ($CH_4 \bullet 6H_2O$), and Blangden's law (Ladd, 1998) to calculate the fusion temperature of water in an electrolyte solution of 3.5 wt% salinity. For Blangden's law, a water cryoscopic constant of 1853 K mol^{-1} and a NaCl van't Hoff factor of 2 were considered. The average thickness of the GHSZ in each model cell (Figure 2) was calculated using the different phase boundaries within their valid range of application (Table 1).

2.2 Sedimentation Rate and Particulate Organic Carbon

Two different methods were considered to calculate the sedimentation rate. Method 1 uses the water depth vs sedimentation rate relationship for Holocene sediments from Burwicz et al. (2011), and Method 2 uses an average sedimentation rate from the ratio between the sediment thickness (Whittaker et al., 2013) and the age of oceanic crust (Müller et al., 2008). The data for Method 2 were obtained from The National Oceanographic Data Centre website (*http://www.ngdc.noaa.gov/mgg/sedthick/*; *http://www.ngdc.noaa.gov/mgg/ocean_age/ocean_age_2008.html*), and in the cells where the data were no available, and could not be reliably extrapolated, the sedimentation rate calculated with Method 1 was used. GH would have formed over a period much larger than the Holocene, however, the sedimentation rates from Method 2 are very sparse and excessive interpolation and extrapolation is required. Therefore, in the following sections only the results using Method 1 are presented and discussed. The POC was calculated using the expression proposed by Marquardt et al. (2010) that relates sedimentation rate to POC. We note the problematic of using two empirical relationships to transform water depth to POC. However, our calculated average and maximum POC of 1.8 wt% and 2.98 wt% are only slightly higher, and very similar, respectively, than the average and maximum total organic carbon (TOC) of 1.1 wt% and 2.83 wt% obtained from different providences in the Arctic Ocean (Seiter et al., 2004).

3. Results and Discussion

At present, the volume of marine sediments within the GHSZ in the Arctic may be 2.25×10^{15} m^3 (Figure 2a and Table 2) containing between 0.28 and 541 Gt of carbon (Figure 2c and Table 2). Based on Wallmann's et al. (2012) transfer equation for steady-state compaction and a slight modification of Burwicz et al. (2013) to consider Quaternary accumulation rates, Kretschmer et al. (2015) estimated a present day volume of the GHSZ of 3.80×10^{15} m^3 containing 116 Gt of carbon. Our lower value of GH inventory using the same transfer function as Kretschmer et al. (2015) is likely because they estimated a larger volume of the GHSZ and assumed higher sedimentation rates at continental slopes (between 200-500 m water depth).

Besides, they used a thermal conductivity of 1.5 W m^{-1} K^{-1}, which may be too high for the shallow sediments (e.g. Wallmann et al., 2012). However, our upper bound value of the GH inventory is an order of magnitude larger than their estimated value (Table 2) due to the contribution of the 0.01 cm yr^{-1} upward advective fluid flow (FF) into the GHSZ, which increases the methane input into the GHSZ. Fluid flow velocities of ~0.02 cm yr^{-1} are consistent with published values in active margins (e.g., Buffet and Archer, 2004).

For each model cell, the average GH saturation (S_h) can be estimated by introducing into Eq. (2) the estimated thickness of the GHSZ (H_{GHSZ} in m) and the carbon mass (m_C in kg) calculated with any of the transfer equations explained above, and assuming the average porosity of the sediments located within the GHSZ (ϕ), the hydrate density (ρ_{GH} in kg m^{-3}), and the hydration number (N_h).

$$S_h = m_C \cdot \left(\phi \frac{M_C}{N_h \cdot M_{H2O} + M_{CH4}} \rho_{GH} \cdot H_{GHSZ} \cdot A \right)^{-1} \quad (2)$$

In Eq. (2) M_C is the molecular mass of carbon, M_{H2O} is the molecular mass of water, and M_{CH4} is the molecular mass of methane. Assuming a ϕ of 0.5, a structure 1 ρ_{GH} of 912 kg m^{-3}, a N_h of 6, and using Eq. (1) with an upward fluid flow of 0.01 cm yr^{-1}, the associated average GH saturation below the sediments in the entire Arctic Ocean is 0.25% (Figure 2d). This average GH saturation is significantly lower than the saturation inferred offshore west of Svalbard at water depths between ~1285-1500 m of 6-13% (Chabert et al., 2011) and of ~10% in the Beaufort Sea (Andreassen et al., 1997). Besides, we estimate much lower saturations at these two Arctic sites (Figure 2d). One possible explanation for this discrepancy is the underestimation of the sediment accumulation at water depths where hydrate is stable. In fact, two contrasting models exist in the central Arctic Ocean, one suggesting mm kyr^{-1}-scale sedimentation rates during Plio-Pleistocene times and other suggesting cm kyr^{-1}-scale sedimentation rates over millions of years (Backman et al., 2004). Increasing by an order of magnitude the sedimentation rates shown in Figure 3b and keeping the upward FF constant at 0.01 cm yr^{-1}, results in an Arctic average hydrate saturation of 0.2%. For a fix FF, increasing the SR tends to reduce the GH inventory (Piñero et al., 2013). Using Holocene sedimentation rates (Fig. 3b) and to obtain GH saturations between ~1-10%, an equivalent FF (FFe) contribution of 0.02-0.04 cm yr^{-1} is required. Here we have introduced the concept of FFe because Eq. (1) does not consider the free methane gas ascent to the GHSZ. Therefore, these fluid velocities should be interpreted only as equivalent velocities of a methane-saturated fluid. These relatively high FFe velocities suggest that the contribution from particulate organic

carbon and upward fluid flow generated only by steady state mechanical compaction are not enough to explain the geophysical-inferred GH saturations in several places in the Arctic. Other thermogenic and/or biogenic deep sources of carbon-rich fluids may exist and play a dominant role in fuelling Arctic marine GH. This result supports the idea of the important role played by deep buried carbon in cold seeps (Boetius and Wenzhöver, 2013).

One of the key but less constraint parameters in Eq. (1) is the upward fluid flow from mechanisms other than mechanical compaction (FF). To independently constrain FFe (note that here we use the broader concept of equivalent fluid flow defined above), we can use the GH saturation inferred from seismic (e.g., Chabert et al., 2011) and controlled-sourced electromagnetic data (e.g., Goswami et al., 2015) by combining Eqs. (1) and (2), resulting in Eq. (3). An analysis for different combinations of the parameters SR, H_{GHSZ}, S_h and ϕ was performed to see for which combination of parameters the calculated FFe satisfies the domain conditions defined in Eq. (1). The analysis indicates that for SR between 5-150 cm kyr^{-1}, H_{GHSZ} between 10-550 m, S_h between 0.05-50% and ϕ between 20-70%, the domain defined by the condition $\mathrm{FFe}<0.0001\mathrm{SR}\left(2+\ln\left[\mathrm{POC}\right]\right)$ is only valid for S_h <1%. These low hydrate saturations would unlikely be inferred by current geophysical field techniques, hence Eq. (3) is only sensible in the domain $\mathrm{FFe}\geq 0.0001\mathrm{SR}\left(2+\ln\left[\mathrm{POC}\right]\right)$ and for the parameter range in which this condition is satisfied.

$$\mathrm{FFe}=\left(\left(S_h\cdot\phi\frac{\mathrm{M_C}}{N_h\cdot\mathrm{M_{H2O}}+\mathrm{M_{CH4}}}\rho_{GH}\cdot\mathrm{H_{GHSZ}}\right)\cdot\left(c1\cdot\mathrm{H_{GHSZ}^{c2}}\left(c3+\frac{1}{\mathrm{SR}}\right)c4\cdot\mathrm{POC}^{c6}\right)^{-1}-\frac{\mathrm{POC}}{c4}\right)^{\frac{1}{c5}} \quad (3)$$

$$10\leq \mathrm{H_{GHSZ}}\leq 550\ \mathrm{m}\ ;\ 0.5\leq \mathrm{SR}\leq 150\ \mathrm{cm\ kyr^{-1}}\ ;\ 0.01\leq\alpha\cdot\phi\leq 0.35$$

To study the fate of the Arctic marine GH reservoir, we calculated the increment in sediment temperature driven by a seabed temperature increase of 2°C over 100 yr (inset Figure 1) using a thermal diffusion model and assuming 100% water-saturated sediments. We added this temperature increment to the present-day temperature structure, and under this modified thermal state there is an average reduction of the volume of the GHSZ of 5.4% ($1.2\mathrm{x}10^{14}$ m^3; Table 2). However, a reduction on the volume of the GHSZ is not, necessary, one-to-one equivalent to hydrate dissociation, and a better indicator of the influence of future ocean warming on Arctic marine GH is the associated potential carbon released. Note that we do not make any statement regarding the fate of methane once liberated, which is beyond the scope of this work (see Boetius and Wenzhöver, 2013 for a complete review). For the models where not FF is considered (M^C_1 and M^C_2 in Table 2B), the 5.4% volume reduction of the GHSZ results

in a 96.43 (M^C_1) and 80.28% (M^C_2) reduction in the carbon stored in GH (0.27 Gt C and 1.14 Gt C, respectively). In these models, POC is the only source of carbon, and it is sufficient to form GH only in sediments at relatively shallow water depths (below ~600 m), where the sedimentation rates are high (according to Burwicz et al., 2013 relationship). A 2°C increase over 100 yr is enough to start dissociating the base of the GHSZ at those shallow water depths, and so most of the carbon stored in GH is liberated. Our estimated reduction of the GH inventory using the M^C_1 model is similar to that from Kretschmer et al. (2015) of 0.14±0.01Gt C, which uses the same transfer function and a similar approach to calculate the GHSZ at 2100 but with future seabed temperatures from a coupled ocean-atmosphere-sea ice sea level circulation model. On the contrary, when using the model with a uniform FF of 0.1 cm yr^{-1} the formation of hydrate is dominated by the FF term and hydrate can form on the sediments within the GHSZ below the entire Arctic Ocean (Figure 2C). In these models there is almost a one to one relation between the reduction of the GHSZ and the associated released carbon (M^C_3 in Table 2B).

4. Conclusions

- Accurate estimation of the Arctic marine GH reservoir still remains a challenge. More and better distributed geophysically-inferred GH saturations and an increase in the understanding of the carbon sources reaching the GHSZ are essential to constrain the inputs of state-of-the-art modelling approaches.
- West offshore Svalbard and in the Beaufort Sea, the accumulation of particulate organic carbon alone cannot explain the seismically-inferred GH saturations above 5%, which likely result from the upwards migration of carbon-rich fluids equivalent to 0.02 to 0.04 cm yr^{-1} from other deep sources. This result suggests that the marine GH inventory in the Arctic is probably larger than that recently estimated of 116 Gt of carbon (Kretschmer et al., 2015).
- The present-day Arctic marine GH inventory may be between 0.28-541 Gt of carbon. A 2°C seabed temperature increase over 100 yr may reduce the reservoir by about 88.4% (0.7 Gt C) if particulate organic carbon is the only source, and by about 5.4% (29.7 Gt C) if the main source of carbon is the upwards advection of carbon-rich fluids.

Acknowledgements

This work was partly supported by the European Social Fund, Operational Programme 2007-2013, Objective 2 Regional Competitiveness and Employment, Axis 5 Transnational cooperation, TALENTS FVG Programme (Friuli Venezia Giulia).

We thank The National Oceanographic Data Centre (http://www.nodc.noaa.gov/cgi-bin/OC5/WOA09/woa09.pl) for making available the ocean temperature data, The International Bathymetric Chart of the Arctic Ocean (IBCAO) project (http://www.ngdc.noaa.gov/mgg/bathymetry/arctic/downloads.html) for the bathymetric data, and the Global Heat Flow Database of the International Heat Flow Commission (http://www.heatflow.und.edu/index2.html) for the thermal conductivity data.

References

Andreassen, K., Hart, P.E., MacKay, M., 1997. Amplitude versus offset modeling of the bottom simulating reflection associated with submarine gas hydrates. Marine Geology 137, 25-40, doi: 10.1016/S0025-3227(96)00076-X.

Backman, J., Jakobsson, M., Løvlie, R., Polyak, L., Febo, L.A., 2004. Is the central Arctic Ocean a sediment starved basin? Quaternary Science Reviews 23, 1435-1454, doi: 10.1016/j.quascirev.2003.12.005.

Boetius, A., Wenzhöfer, F., 2013. Seafloor oxygen consumption fuelled by methane from cold seeps. Nature Geoscience 6, 725-734, doi: 10.1038/NGEO1926.

Boswell, R., Collett T., 2006. The gas hydrates resource pyramid, Fire in the Ice, US Department of Energy, Office of Fossil Energy, National Energy Technology Laboratory 6(3), 5-7.

Buffett, B., Archer, D., 2004. Global inventory of methane clathrate: sensitivity to changes in the deep ocean. Earth and Planetary Science Letters 227, 185-199, doi: 10.1016/j.epsl.2004.09.005.

Burwicz, E.B., Ruepke, L., Wallmann, K., 2011. Estimation of the global amount of submarine gas hydrates formed via microbial methane formation based on numerical reaction-transport modeling and a novel parameterization of Holocene sedimentation. Geochimica et Cosmochimica Acta 75, 4562-4576, doi: 10.1016/j.gca.2011.05.029.

Chabert, A., Minshull, T.A., Westbrook, G.K., Berndt, C., Thatcher, K.E., Sarkar, S., 2011. Characterization of a stratigraphically constrained gas hydrate system along the western continental margin of Svalbard from ocean bottom seismometer data. Journal of Geophysical Research: Solid Earth (1978-2012) 116, B12102, doi: 10.1029/2011JB008211.

Dickens, G.R., Quinby-Hunt, M.S., 1994. Methane hydrate stability in seawater. Geophysical Research Letters 21, 2115-2118, doi: 10.1029/94GL01858.

Dickens, G.R., Quinby-Hunt, M.S., 1997. Methane hydrate stability in pore water: A simple theoretical approach for geophysical applications. Journal of Geophysical Research: Solid Earth 102, 773-783, doi: 10.1029/96JB02941.

Goswami, B.K., Weitemeyer, K.A., Minshull, T.A., Sinha, M.C., Westbrook, G.K., Chabert, A., Henstock, T.J., Ker, S., 2015. A joint electromagnetic and seismic study of an active pockmark within the hydrate stability field at the Vestnesa Ridge, West Svalbard margin. Journal of Geophysical Research: Solid Earth, n/a-n/a.

Hunter, S. J., D. S. Goldobin, A. M. Haywood, A. Ridgwell, and J. G. Rees (2013), Sensitivity of the global submarine hydrate inventory to scenarios of future climate change, Earth and Planetary Science Letters, 367(0), 105-115, doi: 10.1016/j.epsl.2013.02.017.

Kretschmer, K., Biastoch, A., Rüpke, L., Burwicz, E., 2015. Modeling the fate of methane hydrates under global warming. Global Biogeochemical Cycles 29, 610-625, doi: 10.1002/2014GB005011.

Kvenvolden, K., Ginsburg, G., Soloviev, V., 1993. Worldwide distribution of subaquatic gas hydrates. Geo-Marine Letters 13, 32-40, doi: 10.1007/BF01204390.

Ladd, M., 1998. Introduction to Physical Chemistry. Cambridge University Press, Cambridge, UK.

Lu, Z., Sultan, N., 2008. Empirical expressions for gas hydrate stability law, its volume fraction and mass-density at temperatures 273.15 K to 290.15 K. Geochemical Journal 42, 163-175, doi: 10.2343/geochemj.42.163.

Marquardt, M., Hensen, C., Piñero, E., Wallmann, K., Haeckel, M., 2010. A transfer function for the prediction of gas hydrate inventories in marine sediments. Biogeosciences 7, 2925-

2941, doi: 10.5194/bg-7-2925-2010.

Moridis, G.J., Kowalsky, M.B., Pruess, K., 2008. TOUGH+HYDRATE v1.0 user's manual: A code for the simulation of system behaviour in hydrate-bearing geologic media, LBNL-149E, Lawrence Berkeley Natl. Lab., Berkeley, California.

Müller, R.D., Sdrolias, M., Gaina, C., Roest, W.R., 2008. Age, spreading rates, and spreading asymmetry of the world's ocean crust. Geochemistry, Geophysics, Geosystems 9, n/a-n/a, doi: 10.1029/2007GC001743.

Piñero, E., Marquardt, M., Hensen, C., Haeckel, M., Wallmann, K., 2013. Estimation of the global inventory of methane hydrates in marine sediments using transfer functions. Biogeosciences 10, 959-975, doi: 10.5194/bg-10-959-2013.

Seiter, K., Hensen, C., Schröter, J., Zabel, M., 2004. Organic carbon content in surface sediments-defining regional provinces. Deep Sea Research Part I: Oceanographic Research Papers 51, 2001-2026.

Sloan, E.D., Koh, C., 2008. Clathrate hydrates of natural gases, third ed. CRC press, Boca Raton, FL.

Talley, L.D., Pickard, G.L., Emery, W.J., Swift, J.H., 2011. Descriptive physical oceanography: an introduction, Sixth ed. Academic Press.

Tishchenko, P., Hensen, C., Wallmann, K., Wong, C.S., 2005. Calculation of the stability and solubility of methane hydrate in seawater. Chemical Geology 219, 37-52, doi: 10.1016/j.chemgeo.2005.02.008.

Wallmann, K., Piñero, E., Burwicz, E., Haeckel, M., Hensen, C., Dale, A., Ruepke, L., 2012. The Global Inventory of Methane Hydrate in Marine Sediments: A Theoretical Approach. Energies 5, 2449-2498, doi: 10.3390/en5072449.

Whittaker, J.M., Goncharov, A., Williams, S.E., Müller, R.D., Leitchenkov, G., 2013. Global sediment thickness data set updated for the Australian-Antarctic Southern Ocean. Geochemistry, Geophysics, Geosystems 14, 3297-3305, doi: 10.1002/ggge.20181.

Tables

Table 1. Gas hydrate stability curves and their temperature and salinity ranges of valid application.

Reference	Temperature [K]	Salinity [wt%]
Dickens and Quinby-Hunt (1994); Eq. 1	271.93-285.14	3.35
Dickens and Quinby-Hunt (1997); Table 4	274.47-283.73	0-6
Sloan (1998); K_{vsi}-Method; Eq. 4.2	273.15-300	0
Tischenko (2005); Eq. 24	273-293	0-7
Lu and Sultan (2008); Eq. 8	273.15-290.15	$0<S\leq13.966$
Moridis et al. (2008); Fig. 2.1	160-320	0

Table 2. A) Volume of the gas hydrate stability zone (GHSZ) and mass carbon stored in Arctic marine gas hydrate bearing sediments (GHBS). The relationships used are: M^C_1 and M^C_2 from Wallmann et al. (2012) for normally and fully compacted sediments, respectively, and M^C_3 from Piñero et al. (2013) for an upwards advective flow velocity of 0.01 cm yr^{-1}. In M^C_1, M^C_2, and M^C_3 the first number is the mass carbon calculated using the sedimentation rates from Method #1 and the second using Method #2. B) Change in the volume of the GHSZ and in the mass of carbon due to ocean warming. Notation: P_0 seabed pressure; T_0, seabed temperature; TG, thermal gradient; $K_{th,}$ thermal conductivity;

A) Carbon Stored in Arctic Marine GHBS [Gt]

	$V^{GHSZ\,(1)}$ [$x10^{15}$ m^3]	M^C_1	M^C_2	M^C_3 (0.01 cm yr^{-1})
Models at Present Day				
Base	2.23	0.28/0.13	1.42/0.62	540.77/1179.10
Base with +30% P_0	2.59	2.74/0.93	7.37/2.36	645.88/1420.07
Base with -30% P_0	1.81	$1x10^{-4}$/0.03	0.03/0.21	414.72/891.02
Base with +30% TG	1.72	0.19/0.09	0.99/0.42	355.79/775.15
Base with -30% TG	3.19	0.62/0.29	2.81/1.20	950.45/2070.70
Base with +30% T_0	2.18	0.22/0.11	1.23/0.55	525.07/1143.00
Base with -30% T_0	2.29	0.45/0.20	1.91/0.79	554.89/1210.03
Models at 2100 CE				
Base with K_{th} of 1.0 W m^{-1} K^{-1}	2.12	0.01/0.04	0.28/0.28	514.83/1115.05
Base with K_{th} of 1.4 W m^{-1} K^{-1}	2.1	0.01/0.04	0.27/0.28	508.37/1100.70

B) Change in Carbon Stored in Arctic Marine GHBS [%]

	$V^{GHSZ\,(1)}$ [$x10^{15}$ m^3]	M^C_1	M^C_2	M^C_3 (0.01 cm yr^{-1})
Models at Present Day[(1)]				
Base				
Base with +30% P_0	16.14	878.57/615.38	419.01/280.65	19.44/20.44
Base with -30% P_0	-18.83	-99.96/-76.92	-97.89/-66.13	-23.31/-24.43
Base with +30% TG	-22.87	-32.14/-30.77	-30.28/-32.26	-34.21/-34.26
Base with -30% TG	43.05	121.43/123.08	97.89/93.55	75.76/75.62
Base with +30% T_0	-2.24	-21.43/-15.38	-13.38/-11.29	-2.90/-3.06
Base with -30% T_0	2.69	60.71/53.85	34.51/27.42	2.61/2.62
Models at 2100 CE[(2)]				
Base with K_{th} of 1.0 W m^{-1} K^{-1}	-4.93	-96.43/-69.23	-80.28/-54.84	-4.80/-5.43
Base with K_{th} of 1.4 W m^{-1} K^{-1}	-5.83	-96.43/-69.23	-81.69/-54.84	-5.99/-6.65

(1) $\Delta V^{GHSZ}_{t0} = (V^{GHSZ}_{t0} - V^{GHSZ}_{0,t0}) / V^{GHSZ}_{0,t0}$; $\Delta M^C_{t0} = (M^C_{t0} - M^C_{0,t0}) / M^C_{0,t0}$

(2) $\Delta V^{GHSZ}_{t0+100} = \left(V^{GHSZ}_{0,t0+100} - V^{GHSZ}_{0,t0}\right) / V^{GHSZ}_{0,t0}$; $\Delta M^C_{t0+100} = \left(M^C_{0,t0+100} - M^C_{0,t0}\right) / M^C_{0,t0}$

Figures

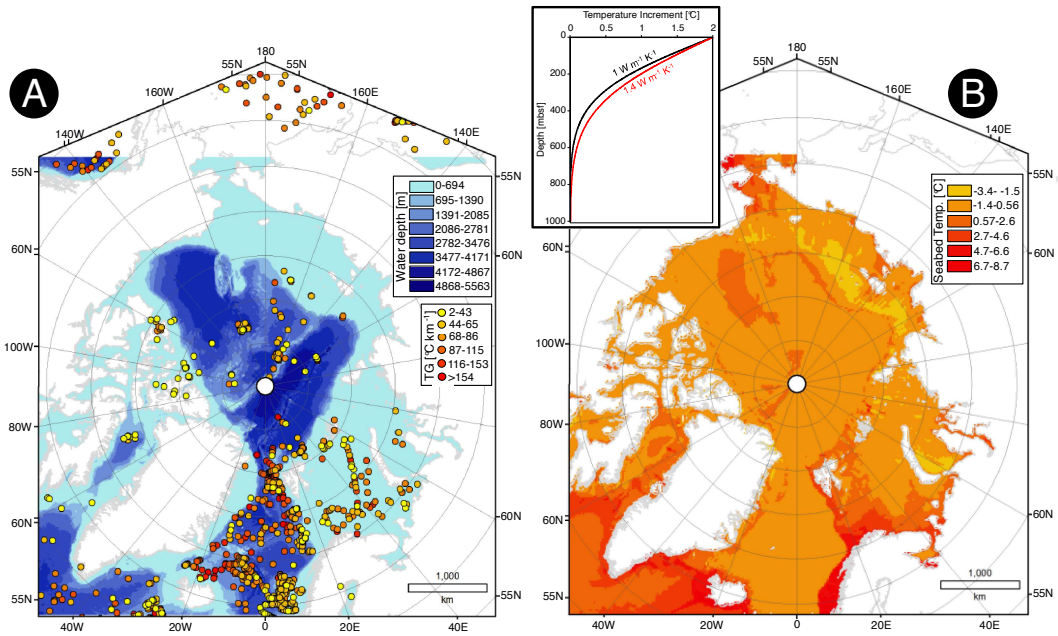

Figure 1: A) Bathymetric map of the Arctic Ocean (http://www.ngdc.noaa.gov/mgg/bathymetry/arctic/downloads.html) with geothermal gradient data overlapped (http://www.heatflow.und.edu/index2.html). B) Seabed temperature data (http://www.nodc.noaa.gov/cgi-bin/OC5/WOA09/woa09.pl). The inset shows the temperature increment in the 100% water saturated sediments driven by a seabed temperature increase of 2°C over 100 yr.

Figure 2: A) Present day average depth of the base of the gas hydrate stability zone (GHSZ) calculated using six different methane hydrate phase boundaries (Dickens and Quinby-Hunt, 1994, 1997; Distribution Coefficient Method or K_{vsi}-Method, Sloan and Koh, 2008; Moridis et al., 2008; Tischenko et al., 2005; Lu and Sultan, 2008) and assuming 3.5 wt% salinity and steady state conditions. B) Holocene sedimentation rate calculated using the water depth vs sediment accumulation relationship from Burwicz et al. (2011). C) Mass of carbon stored in GH estimated using Piñero's et al. (2013) transfer function and assuming a fluid flow of 0.01 cm yr^{-1} and D) associated GH concentration assuming an average porosity of the sediments within the GHSZ of 0.5, a hydrate density of 912 kg m^{-3}, and a hydration number of 6.